J. Fluid Mech. (1973), *vol.* 57, *part* 2, *pp.* 381–400
Printed in Great Britain

Convection in a rotating annulus uniformly heated from below. Part 2. Nonlinear results

By PETER A. GILMAN

Advanced Study Program, National Center for Atmospheric Research,† Boulder, Colorado

(Received 1 May 1972)

Davies-Jones & Gilman (1971) reported in this *Journal* on a linear stability analysis and second-order initial-tendency calculation for thermal convection in a thin rotating annulus heated uniformly from below. The present work gives extensive numerical calculations for an annulus model with realistic laboratory boundary conditions which extends the previous work into the finite amplitude range. The model allows the mode with the longitudinal wavenumber predicted to occur at the onset of instability to grow to a finite amplitude and induce secondary axisymmetric differential rotation and meridional circulation through its Reynolds and thermal stresses, these circulations in turn modifying the forcing cells. No higher harmonics are allowed. The Boussinesq equations for the fundamental mode and secondary circulations are solved on a staggered finite-difference grid in the annulus cross-section, mostly following the scheme laid out by Williams (1969).

Stationary convection is studied for Taylor numbers $T < 3 \times 10^3$. The profile predicted for the mean circulations in the earlier analysis, that of fast rotation in the outer half, slow rotation in the inner half of the annulus (except at very high Prandtl number), together with a four-celled meridional circulation, is confirmed. For a given Taylor number T, the differential-rotation energy peaks relative to the cell energy at a modest Prandtl number P somewhat less than unity, and its production is driven mostly by the Reynolds stresses in the cells. Meridional circulation is driven by potential-energy conversion at high P and by Reynolds stresses at low P, but retains the same form for all P with increased amplitude relative to the cells at low P. For Rayleigh numbers R a given percentage above the critical value R_c, the differential-rotation energy increases like T, while the meridional circulation remains nearly constant. For given P and T differential-rotation relative energy peaks at modest R/R_c, while the meridional circulation continues to increase. The induced differential rotation tends to distort the cell boundaries from tilted straight lines produced by Coriolis forces into S shapes qualitatively like the profile of differential rotation itself.

One example of nonlinear overstable convection is given. The induced differential rotation has time-independent and oscillatory parts. The redistribution of momentum is carried out by periodically reversing horizontal and vertical Reynolds stresses.

† The National Center for Atmospheric Research is sponsored by the National Science Foundation.

1. Introduction

In an earlier paper of the same title (hereafter referred to as I) Davies-Jones & Gilman (1971) presented a linear stability analysis for thermal convection in a thin rotating annulus uniformly heated from below with cross-section of order unity. The linear stability solutions were used to calculate initial second-order tendencies due to products of perturbation variables. These calculations showed that in general a differential rotation and meridional circulation, driven by Reynolds and thermal stresses in the cells, should be expected to develop. This paper reports nonlinear numerical calculations of the form and magnitude of these circulations and their interaction with the cells that force them, for both stationary and overstable convection.

For stationary convection, I predicts the differential rotation to be positive (faster than the rotation rate of the annulus walls) in the outer half of the cross-section and negative in the inner half (see figure 1 (*a*)), except at high Prandtl number. The meridional circulation has four cells, two above two in the cross-section, with rising motion near the centre of the upper half and sinking motion near the centre of the lower half (see figure 1 (*b*)). The horizontal and vertical momentum transport that produces the initial differential rotation is shown in figures 1 (*c*) and (*d*) respectively. Cell vertical transport takes momentum from the middle of the inner half of the annulus, and this is then transported horizontally across to the outer half, where it is reconcentrated about the middle z level. The meridional circulation, through Coriolis forces, reinforces the vertical transport process.

As shown in I, the Reynolds stresses driving the differential rotation arise directly from the effect of Coriolis forces on the transverse rolls of the non-rotating case. These produce an immediate correlation between the zonal flow u_1 and the radial flow v_1 in the cells, which in turn, through the conservation of mass equation, leads to correlations of u_1 with the vertical motion w_1, and finally of v_1 with w_1. (For a typical cell pattern in the rotating case see figure 5.) For the overstable case, the form of the mean circulations were not deduced in I, but it was noted they would be more complicated.

At high Prandtl number P with stationary convection a different differential rotation is produced from that shown in figure 1, for which the inner and outer halves of the annulus rotate at the same average rate. This differential rotation arises only from the action of Coriolis forces on the meridional circulation, which speed up the mid-levels of the outer half of the annulus and slow down the regions near the top and bottom, and produce exactly the opposite pattern for the inner half of the annulus.

2. Formulation of the problem and the method of solution

In terms of the Rayleigh number R, Taylor number T, and Prandtl number P, we seek answers to four questions.

(i) What kind of differential rotation and meridional circulation are produced in the nonlinear case?

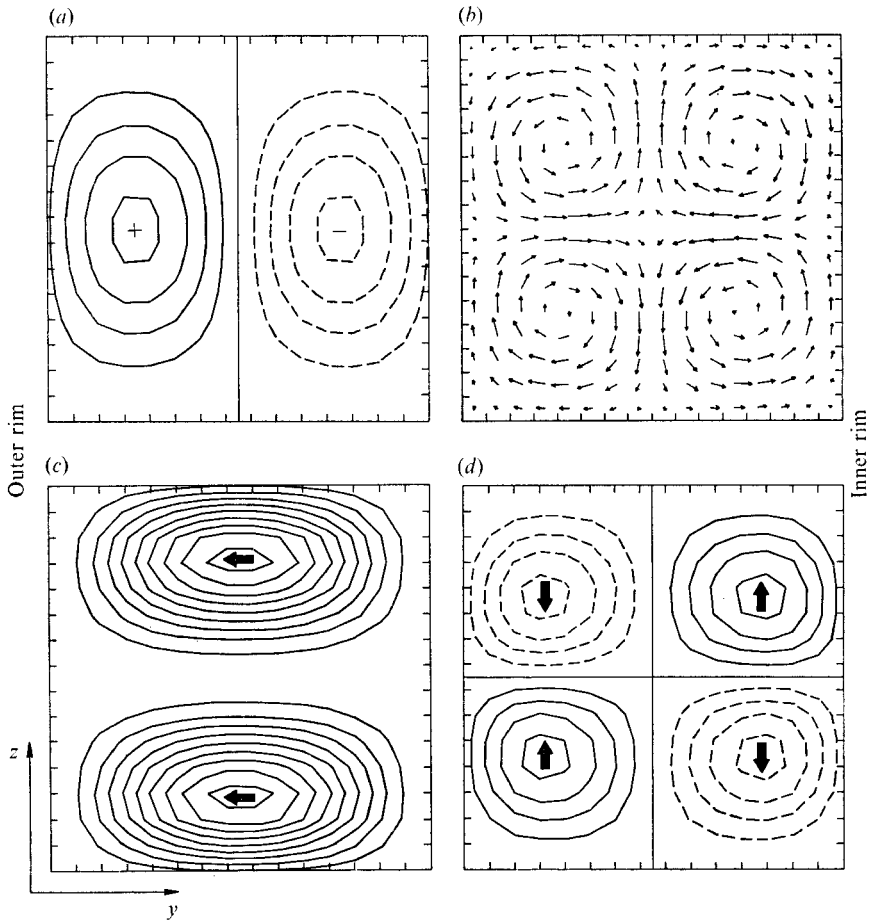

FIGURE 1. Annulus cross-section for stationary convection showing general form of (*a*) induced differential rotation, (*b*) meridional circulation, (*c*) cell horizontal transport of x momentum and (*d*) cell vertical transport of x momentum predicted by I and confirmed in this paper.

(ii) How *much* circulation is produced, compared with that in the forcing cells?

(iii) How are these circulations maintained against dissipation by friction?

(iv) How do they react back on the convective cells which produced them?

As was mentioned in the introduction, paper I, through an initial-tendency calculation from second-order correlation of perturbation quantities, gave some indication of what kind of circulations would be induced, a little information on how they would be maintained, but no indication of how large they would be or how they would modify the cells.

R, T and P are defined in the same manner as in I, namely,

$$R = g\alpha\Delta\theta d^3/\kappa\nu, \quad T = 4\Omega^2 d^4/\nu^2, \quad P = \nu/\kappa,$$

in which g is gravity, α the coefficient of volume expansion, $\Delta\theta$ the total temperature difference across the depth d of the annulus, κ is the thermal diffusivity,

ν the kinematic viscosity and Ω the rotation rate of the annulus. The equations to be solved are the standard Boussinesq convection equations in Cartesian co-ordinates as given, for example, in I. We solve these equations for a thin annulus of square cross-section, with reasonable laboratory boundary conditions, namely, no-slip conditions (zero velocity relative to the rotating frame) on the top, bottom and sides, with perfectly thermally conducting top and bottom (fixed temperature) and perfectly insulating sides. (In I, for mathematical reasons, we assumed a stress-free top and bottom.) Our co-ordinates are x, parallel to the annulus walls; y, the inward radial; and z, upwards; with corresponding velocities u, v and w. Thus the cross-section of the annulus lies in the y, z plane.

The basic solution scheme is as follows. First, we take Fourier transforms with respect to x of the equations of motion, thermodynamics and continuity and then retain only the wavenumber 0 (the mean circulations) plus a single longitudinal wavenumber k. All interactions which produce higher harmonics are discarded. We then temporarily suppress all nonlinear terms and solve the linear stability equations in y, z and t numerically for the cell variables u_1, v_1, w_1, θ_1 and π_1 to find the critical Rayleigh number R_c and longitudinal wavenumber k_c as functions of P and T. We then allow the convective mode with wavenumber $k = k_c$ to grow to finite amplitude, produce by the nonlinear stresses a mean flow (u_0, v_0, w_0) and interact with it. The y, z profiles and the amplitudes of the cells, then, are allowed to change owing to nonlinear effects, but the longitudinal wavenumber remains fixed. It is important to stress that effectively only the higher harmonics *in the x co-ordinate* are suppressed. With the finite differences in y and z, clearly higher harmonics in these co-ordinates are allowed to develop. In other words, the shears in the induced mean flows, together with distortions of the basic temperature profile in y and z, are allowed to feed back on the fundamental convection mode. As such, this is more general than the 'shape assumption' introduced by Stuart (1958) for the rotating-cylinder problem. Nevertheless, suppression of x harmonics of the fundamental wavenumber k_c and consequently their reaction upon the fundamental, while retaining the mean state, is to a fair degree arbitrary. Its validity can really be tested only by numerical integrations which include one or more higher harmonics. We may attempt this for certain cases in the near future.

The numerical scheme used is basically similar to that outlined by Williams (1969), with the following modifications. The pressure equations were solved in early runs by over-relaxation and later by direct matrix inversion using Chileski decomposition, rather than by fast Fourier transforms. Certain symmetries are invoked along the bisectors of the cross-section in order to reduce the amount of computation. These are consistent with the most unstable linear solutions and if imposed initially are preserved by the nonlinear equations, so no loss of generality is involved. Otherwise, the same staggered grid that conserves energy in the nonlinear terms is used, as well as leap-frog time advancement. Calculations were performed for 10×10 and 16×16 intervals in the cross-section, with the time step chosen small enough to avoid the various computational instabilities discussed by Williams.

3. Kinetic-energy diagnostic equations

In analysing the nonlinear results, we make extensive use of kinetic-energy equations for the differential rotation u_0, and for the mean meridional circulation (v_0, w_0). These can be derived from the equations of motion for these variables, using the boundary conditions to eliminate boundary fluxes. In condensed notation, the differential-rotation kinetic-energy equation is given by

$$\partial U_0^2/\partial t = A + B + C - D, \tag{1}$$

and the meridional-circulation kinetic-energy equation by

$$\partial(V_0^2 + W_0)^2/\partial t = -A + E + F - G, \tag{2}$$

in which

$$\left.\begin{aligned}
&U_0^2 \equiv \iint \frac{u_0^2}{2}\,dy\,dz, \quad V_0^2 + W_0^2 \equiv \iint \frac{v_0^2 + w_0^2}{2}\,dy\,dz,\\
&A \equiv PT^{\frac{1}{2}} \iint u_0 v_0\,dy\,dz, \quad B \equiv \iint (u_1 v_1)_0 \frac{\partial u_0}{\partial y}\,dy\,dz,\\
&C \equiv \iint (u_1 w_1)_0 \frac{\partial u_0}{\partial z}\,dy\,dz, \quad D \equiv P \iint \left[\left(\frac{\partial u_0}{\partial y}\right)^2 + \left(\frac{\partial u_0}{\partial z}\right)^2\right] dy\,dz,\\
&E \equiv PR \iint w_0 \theta_0\,dy\,dz,\\
&F \equiv \iint \left[(v_1 w_1)_0 \left(\frac{\partial v_0}{\partial z} + \frac{\partial w_0}{\partial y}\right) + (v_1^2)_0 \frac{\partial v_0}{\partial y} + (w_1^2)_0 \frac{\partial w_0}{\partial z}\right],\\
&G \equiv P \iint \left[\left(\frac{\partial v_0}{\partial y}\right)^2 + \left(\frac{\partial v_0}{\partial z}\right)^2 + \left(\frac{\partial w_0}{\partial y}\right)^2 + \left(\frac{\partial w_0}{\partial z}\right)^2\right].
\end{aligned}\right\} \tag{3}$$

The integrals are over the cross-section of the annulus, and for unit length in the x direction. All variables are dimensionless, with lengths scaled by d, time scaled by d^2/κ, velocities by κ/d and temperature by $\Delta\Theta$.

From (1)–(3) we see that the differential-rotation energy U_0^2 can be maintained against frictional dissipation D in basically two ways. One is by Coriolis forces acting on the meridional circulation, A. The second is by horizontal and vertical Reynolds stresses from the convective cells, $(u_1 v_1)_0$ and $(u_1 w_1)_0$ respectively, through B and C. To make the kinetic energy of differential rotation increase, these stresses must selectively transport u momentum from regions of small (or negative) u_0 to regions of large u_0, that is, *up* the gradient of momentum. This is the opposite of a frictional decay process.

The meridional circulation energy $V_0^2 + W_0^2$ can be maintained against dissipation G in three ways: (*a*) by Coriolis forces acting on the differential rotation through $-A$; (*b*) by conversion of potential energy due to rising warm fluid and sinking of cold represented by E; and (*c*) by the stresses $(v_1 w_1)_0$, $(v_1^2)_0$ and $(w_1^2)_0$ transporting momentum against the gradients of v_0 and w_0, as contained in F. Of course Coriolis forces acting on the mean motion simply convert one component of energy to another, but cannot contribute any net energy to the sum $U_0^2 + V_0^2 + W_0^2$.

If the Reynolds stresses supply energy to the mean circulations, this energy must come from the kinetic energy of the cells themselves. This would be reflected

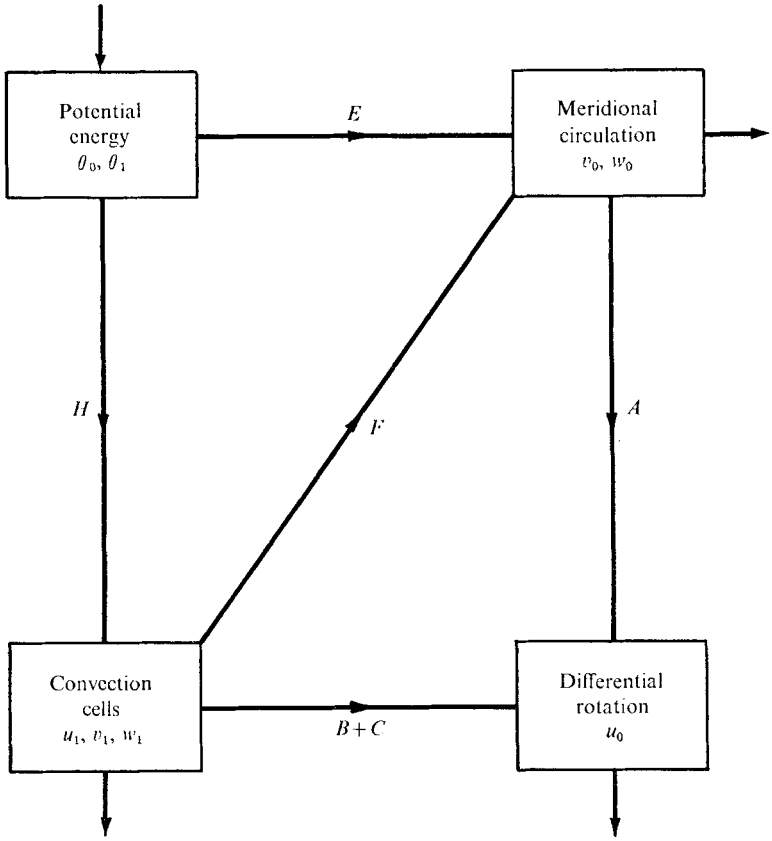

FIGURE 2. Schematic diagram of nonlinear energy conversions possible in model, with arrows indicating usual direction of this conversion.

in a cell kinetic-energy equation (not written down), in which B, C and F appear with the opposite sign from (1) and (2). The principal maintenance of the cells is by the rising of warm fluid and sinking of cold in them. In our calculations it turns out that only a relatively small fraction of the energy converted in this way is needed for the stresses which maintain the differential rotation and meridional circulations. Most of it goes directly into dissipation.

The energy conversion processes possible in the model are summarized graphically in figure 2. The arrows correspond to the sense of conversion which actually occurs in virtually all cases examined.

4. Linear instability results

The critical Rayleigh number R_c and longitudinal wavenumber k_c for linear instability are shown in figures 3 (*a*) and (*b*). For stationary convection, the points on these curves are found by integration of the equations at each T for several wavenumbers at the two values of R which are estimated initially to straddle the stability boundary. The integration is carried on long enough to establish a constant growth rate, from which the stability boundary (zero growth rate)

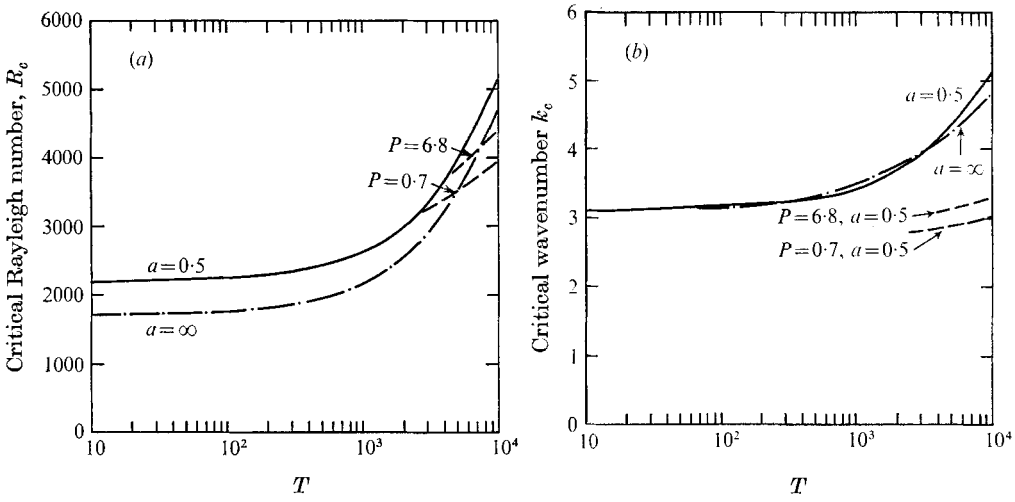

FIGURE 3. (*a*) Critical Rayleigh number and (*b*) critical x wavenumber as function of Taylor number T for onset of stationary convection (solid and dot-dashed lines) and overstable convection (dashed lines). $a = 0{\cdot}5$ corresponds to annulus with square cross-section, $a = \infty$ to infinite plane case with same boundary conditions at top and bottom.

is found by interpolation. For overstable convection, enough cases are run to find a set of (R, k) pairs at which the solutions oscillate without growth or decay. This must be done because there are two overstable modes excited at the same Rayleigh number, which propagate in opposite directions around the annulus, undergoing linear mutual interference that is periodically constructive and destructive.

In figure 3(*a*), the stability boundary for the annulus of square cross-section is the solid line, which, as in I, is independent of Prandtl number. Boundaries for overstable convection for water ($P = 6{\cdot}8$) and air ($P = 0{\cdot}7$) are shown near the right-hand edge. Corresponding curves for k_c are shown in figure 3(*b*). For comparison, the stationary convection stability boundary without side walls ($a = \infty$) is also shown. From figures 3 we see the following.

(i) Rotation stabilizes the convection, as in the case without side walls; that is R_c increases with T, as does k_c.

(ii) At this aspect ratio, the viscous effects of the side walls are slightly stabilizing for stationary convection.

(iii) Overstability occurs for Prandtl numbers greater than 0·677, which is contrary to the infinite plane case, but similar to the annulus case with free top and bottom (see I).

The structure of the stationary convection is similar to that shown in I, with the cell vertical boundaries turned clockwise from a position perpendicular to the annulus sides (when viewed from above). A typical example of the horizontal planform is shown in figure 4. In these cells horizontal velocity vectors are tilted with respect to longitude such that vectors with a longitudinal component in the same sense as the rotation are pointed towards the outer rim, those with the opposite sense towards the inner rim. This is caused by the Coriolis forces turning

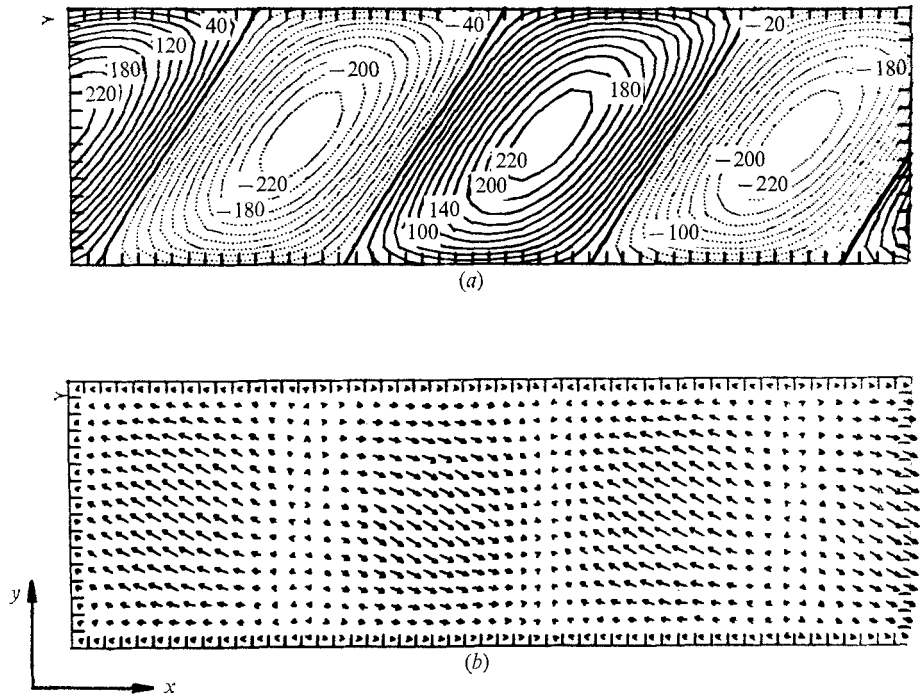

FIGURE 4. Cell structure for typical case with rotation ($T = 10^3, R = 3120, P = 0{\cdot}7, k = 3{\cdot}4$). (*a*) Cell vertical velocities at midlevel of annulus. (*b*) Cell horizontal velocities a quarter of distance up from annulus bottom.

the flow to the right and gives the outward horizontal transport of momentum. The most important difference from the case with a stress-free top and bottom is that here the horizontal velocities in the cells fall to zero at the top and bottom, as well as, by symmetry, at the midlevel.

The overstable convection patterns are time dependent, with the temperature, pressure and vertical motion moving in the prograde sense near the inner rim and the same amount in the retrograde sense in the outer half. This is because the amplitudes of the two overstable modes are individually highly asymmetric about the centre-line of the annulus. The resultant horizontal velocity vectors rotate with time, in a clockwise sense when viewed from above (see figure 5 for an example), which leads to horizontal and also vertical momentum transport which reverse with time. Thus we should expect an oscillatory differential rotation from overstable convection, which is described briefly under the nonlinear results.

5. Nonlinear results

Calculations for stationary convection are reported in §§ 5.1–5.5 below and an example of overstable convection is given in § 5.6. For stationary convection, the numerical solutions always converged to a steady state. The rate of convergence was generally fastest for Prandtl numbers of order unity; as P was decreased the solutions oscillated for longer periods initially. Most cases were run using as

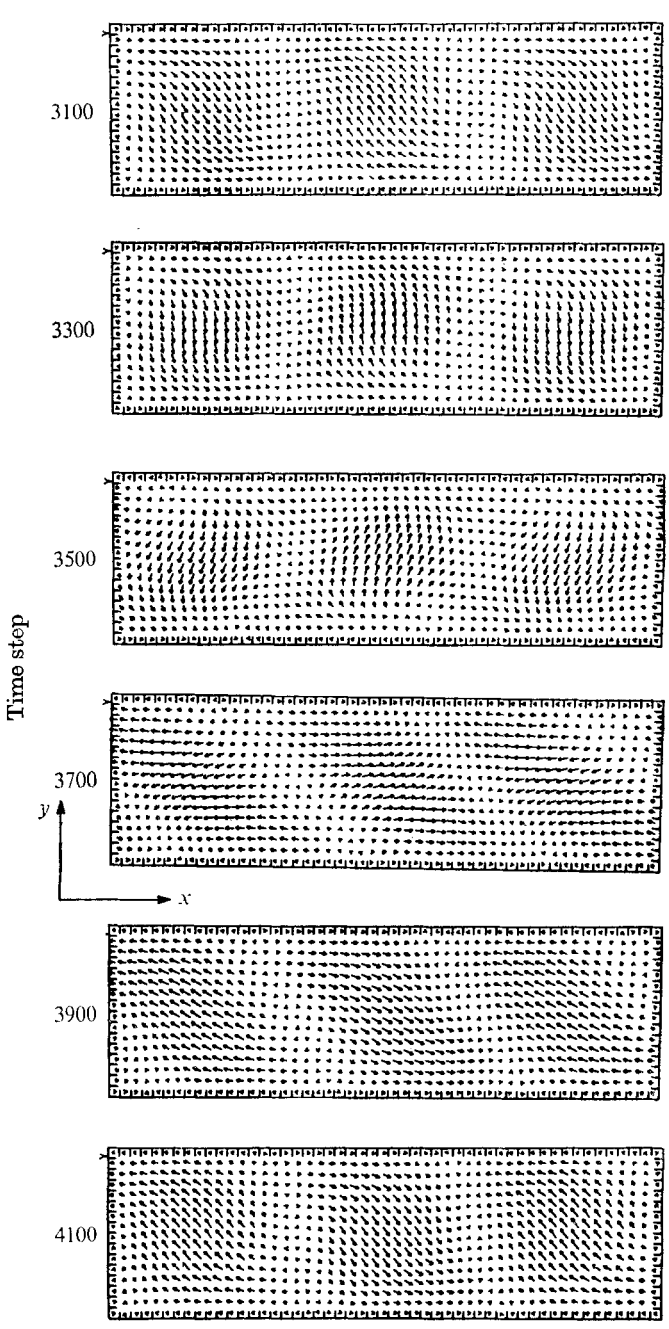

FIGURE 5. Sequence of horizontal velocities through a half-cycle of an overstable convective oscillation, quarter of way up from annulus bottom ($T = 10^4$, $R = 5700$, $P = 0{\cdot}7$, $k = 2{\cdot}9$). Time step here is $4{\cdot}5 \times 10^{-4}$ dimensionless units.

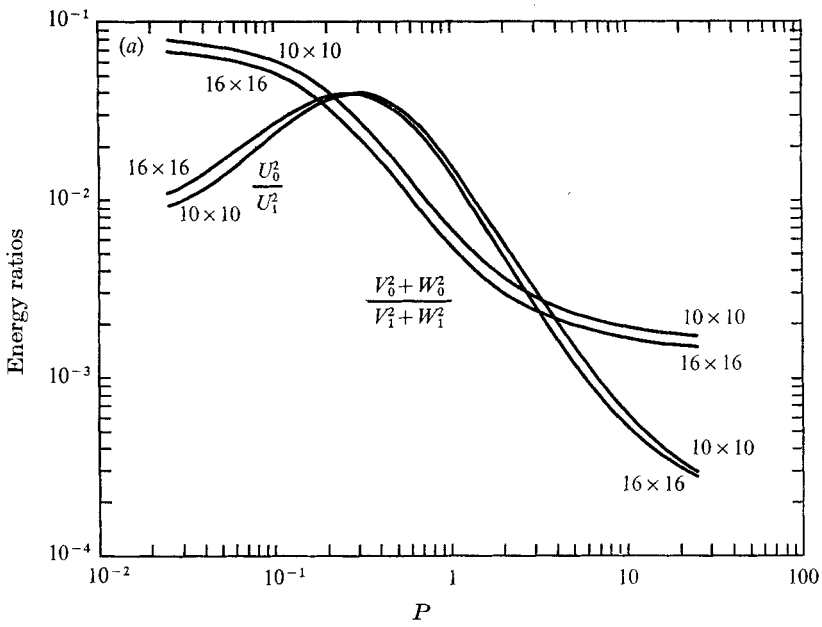

FIGURE 6(a). For legend see facing page.

initial conditions the end result of a previous case nearby in the parameter space. However, as a check on the uniqueness of the results, some cases were run from radically different initial conditions. In all cases studied, the end result was sensibly the same. Fairly close to the critical Rayleigh number, we found that in general the nonlinear solution for the mean circulation forced by stationary convection bore close qualitative resemblance to that predicted in I, except, of course, for effects of the no-slip top and bottom boundary conditions. In that regard, we did not go high enough in T to produce thin Ekman layers at top and bottom.

5.1. *Amplitudes*

The amount of mean circulation produced, we find, varies considerably with P, T and R. Three examples are shown in figures 6(*a*)–(*c*). In each, we have plotted the total energy U_0^2 in the differential rotation and the total energy $V_0^2+W_0^2$ in the meridional circulation, each measured as a ratio with respect to the energies in the corresponding components of motion in the cells.

Figure 6(*a*) gives a typical scan in Prandtl number from 25 to 0·025 at $T = 10^3$, for $R = 1{\cdot}2R_c = 3120$. (Remember that for stationary convection R_c is independent of P.) We see that the differential rotation peaks at an intermediate Prandtl number, between 0·3 and 0·4, while the meridional circulation produced increases monotonically as P is decreased. Some less extensive calculations carried out scanning through P at other values of T and R indicate similar profiles. We note that the maximum differential-rotation energy attained in figure 6(*a*) is only about 4 % of the energy in the same component of motion in the cells, corresponding to an r.m.s. amplitude ratio of roughly 20 %.

One might expect larger ratios to be attained by going to higher R, but at these

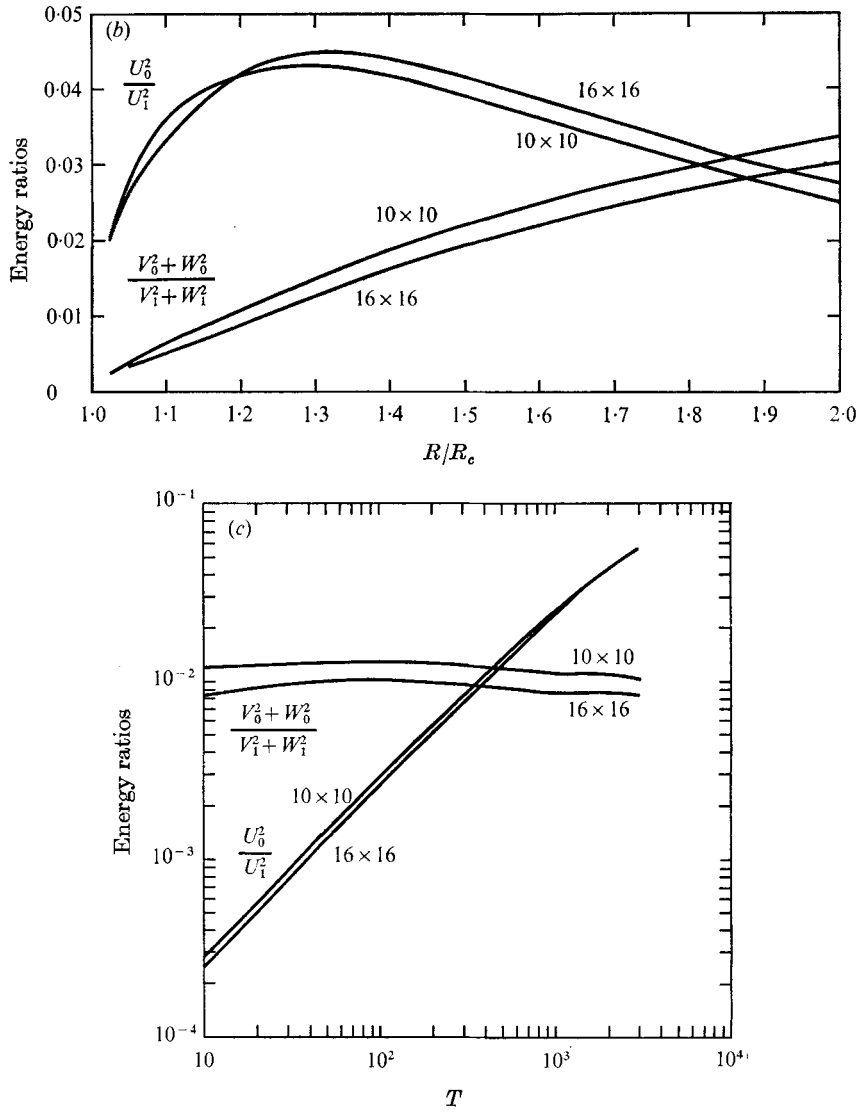

FIGURE 6. Ratios of differential-rotation and meridional-circulation energies (U_0^2 and $V_0^2+W_0^2$, respectively) to corresponding cell energies for 10×10 and 16×16 resolution. (*a*) As functions of Prandtl number; $T = 10^3$, $R = 3120$, $k = 3{\cdot}4$. (*b*) As functions of R/R_c for air ($P = 0{\cdot}7$) at $T = 2000$, $k = 3{\cdot}7$ ($= k_c$). (*c*) As functions of T for $R = 1{\cdot}2R_c(T)$, $P = 0{\cdot}7$ (air), $k = k_c(T)$.

modest Taylor numbers we find that the ratio peaks not too far above the critical value and then falls off again. An example of this is seen in figure 6(*b*), for $P = 0{\cdot}7$ (air), $T = 2000$ and $R \leqslant 2R_c$, for which U_0^2/U_1^2 peaks at about 0·045 for $R/R_c \sim 1{\cdot}35$. By contrast, the meridional-circulation energy continues to rise, through the range, with no peak in sight. The differential rotation and meridional circulation also show markedly different behaviour as T is increased for a given P and $R/R_c(T)$, as may be seen again for air in figure 6 (*c*). The differential-rotation

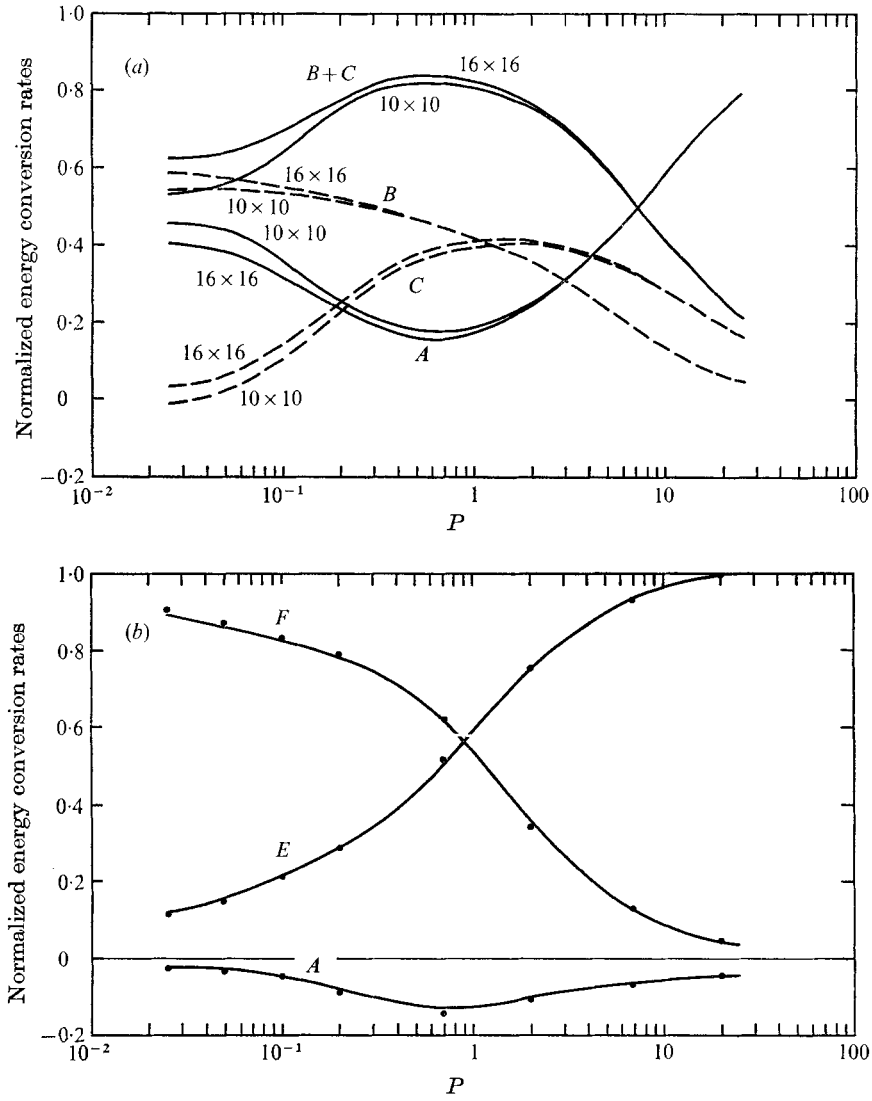

FIGURE 7. Kinetic energy conversion rates for maintenance of (*a*) the differential rotation and (*b*) the meridional circulation as a function of Prandtl number P. See text for definitions. $T = 10^3$, $R = 3120$ ($= 1{\cdot}2R_c$), $k = 3{\cdot}4$. (*b*) ——, 10 × 10; ●, 16 × 16.

energy increases approximately like T, while the meridional circulation is practically constant. There is a very slight change in the slope of the U_0^2/U_1^2 curve at larger T, presumably a small nonlinear reaction of the mean circulation on the cells, modifying slightly their driving action.

5.2. *Kinetic-energy balance*

The means of maintenance of the differential rotation and meridional circulation can easily be found by calculating the kinetic-energy balances implied by (1) and (2) with the left-hand sides equal to zero once the steady state is reached. The

maintenance of the differential-rotation and meridional-circulation amplitudes shown in figure 6 (*a*) is depicted in figures 7 (*a*) and (*b*) respectively. The conversion rates actually plotted are normalized with respect to the dissipation rates D and G. Thus in the steady state, the total energy conversion in each case should add up to $+1{\cdot}0$.

We see from figure 7 (*a*) that the principal mechanisms for maintenance of the differential rotation change markedly with Prandtl number. For $P \gg 1$, the Coriolis forces acting on the meridional circulation do most of the work, and the upgradient transport of momentum by the Reynolds stresses $(u_1 v_1)_0$ and $(u_1 w_1)_0$ is quite weak. This confirms the calculations of earlier tendencies in I. As P is decreased, the Reynolds stresses increase their action relative to the meridional circulation, to such a degree that, at $P = 0{\cdot}7$ (air), the differential rotation is maintained about 80% by the Reynolds stresses, and only 20% by Coriolis forces acting on the meridional circulation. Still further decreases in P draw the stresses down again somewhat, but they appear to be levelling off at the lowest P studied ($0{\cdot}025$). Calculations below this point appeared to be converging to a steady state so slowly as to be impractical. Between the two Reynolds stress effects, the upgradient vertical transports fall off in effectiveness at small P by comparison with the upgradient horizontal transport.

As may be seen in figure 7 (*b*), the meridional circulation is maintained at high Prandtl numbers almost exclusively by conversion from potential energy due to the axisymmetric rising of warm fluid and sinking of cold, while for small P it is maintained entirely by Reynolds stresses, in particular $(w_1^2)_0$. At all P horizontal Coriolis forces extract only a relatively small amount of energy to supply to the differential rotation.

These energy conversion results generally hold for other values of R and T, in the range studied ($R \leqslant 2R_c$). For example, at $P = 0{\cdot}7$, $R = 1{\cdot}2R_c(T)$, the maintenance of both differential rotation and meridional circulation are relatively unchanged as T is increased from zero to the limit of stationary convection. As R/R_c is increased from 1 to 2, the maintenance of differential rotation by vertical momentum transport decreases somewhat and that by Coriolis forces acting on meridional circulation increases a compensating amount. The maintenance of the meridional circulation itself is virtually unchanged.

5.3. *Interpretation of amplitudes and kinetic-energy balance*

At high P, the thermal diffusivity κ is small, relative to ν, so the temperature perturbations θ_1 are large compared with the velocities u_1, v_1 and w_1. Because the velocities are small, owing to large ν, the Reynolds stresses are all very small and play little role in maintenance of secondary circulations. The meridional circulation (v_0, w_0) becomes small compared with (v_1, w_1), because it is driven by the variations in θ_0 produced by the transports $(w_1\theta_1)_0$ and $(v_1\theta_1)_0$ which are small because v_1 and w_1 are small. The differential rotation u_0 is very small compared with the cell velocities because the Reynolds stresses $(u_1 v_1)_0$ and $(u_1 w_1)_0$ are small, the weak meridional circulation (v_0, w_0) produces small Coriolis forces, and the large viscosity depletes u_0.

As P is decreased, the Reynolds stresses, being quadratic in the velocities,

grow faster than the Coriolis forces due to meridional circulation, and the differential rotation becomes maintained more and more by them. As P drops much below unity, the viscous resistance is less, but the relatively large thermal diffusivity now starts to wipe out temperature differences. Consequently, the maintenance of the meridional circulation is more and more by the Reynolds stresses, particularly w_1^2 because it is a maximum in the middle of the annulus cross-section. This is true even without rotation.

It is clear from figures 6(*c*) and 7(*b*) that the meridional circulation is little affected by rotation. The meridional circulation is present principally because the no-slip walls force the thermal and Reynolds stresses to vanish there. Since they are non-zero in the interior, variations with y result and drive (v_0, w_0).

The presence of differential rotation, on the other hand, is tied directly to the rotation. For fixed T, as P decreases, the circulation time in the cells, which is of order d^2/κ or less, becomes short compared with the Coriolis time $(2\Omega)^{-1}$, so the Coriolis forces distort the cells less, and produce smaller Reynolds stresses. The Coriolis forces in the x direction due to the meridional circulation are therefore also less. The vertical Reynolds stress $(u_1 w_1)_0$ falls off even faster than the horizontal component because it is produced only indirectly through continuity of mass while $(u_1 v_1)_0$ is produced directly by Coriolis forces.

The peak in relative energy in the differential rotation as R/R_c increases (figure 6(*b*)) occurs for the same reason. Here the circulation time becomes short compared with the Coriolis time because of increasing velocity amplitude. The meridional circulation keeps on growing because the variations in θ_0 and the stresses v_1^2 and w_1^2 continue to rise, since they do not depend on rotation for their existence.

5.4. *Total heat transport*

The total heat transport (by conduction, in the cells, and the induced meridional circulation) or Nusselt number Nu is shown in figures 8(*a*), (*b*) and (*c*) for the same values P, R/R_c and T, respectively, as for the kinetic energy given in figures 6(*a*), (*b*) and (*c*). The general shape of the Nu curve as a function of P is the same as for the $T = 0$ case (not plotted) except that, for R the same percentage above R_c, Nu is higher in the rotating case except for very small P, for which the influence of T is small. For large P, Nu is independent of P; for small P, Nu falls off sharply as the high thermal diffusivity wipes out temperature gradients. This is similar to the infinite plane case (Rossby 1969). The Nusselt number dependence on R/R_c (figure 8(*c*)) is also similar to the non-rotating case, and the rise of Nu is rather close to the experimental results summarized by Chandrasekhar (1961), indicating that at this aspect ratio the side walls have only modest effects on the heat flux.

It is clear from all of figures 8(*a*), (*b*) and (*c*) that the low resolution (10×10) model consistently overestimates the heat flux. At high P, this is presumably because viscous dissipation in high shear areas, i.e. near the top, bottom and side boundaries, is underestimated, so that larger velocities and therefore heat transport are allowed. At small P, the thermal diffusion which would tend to reduce buoyancy forces and heat transports is underestimated. In terms of percentages, these low estimates are more serious than in the case of the

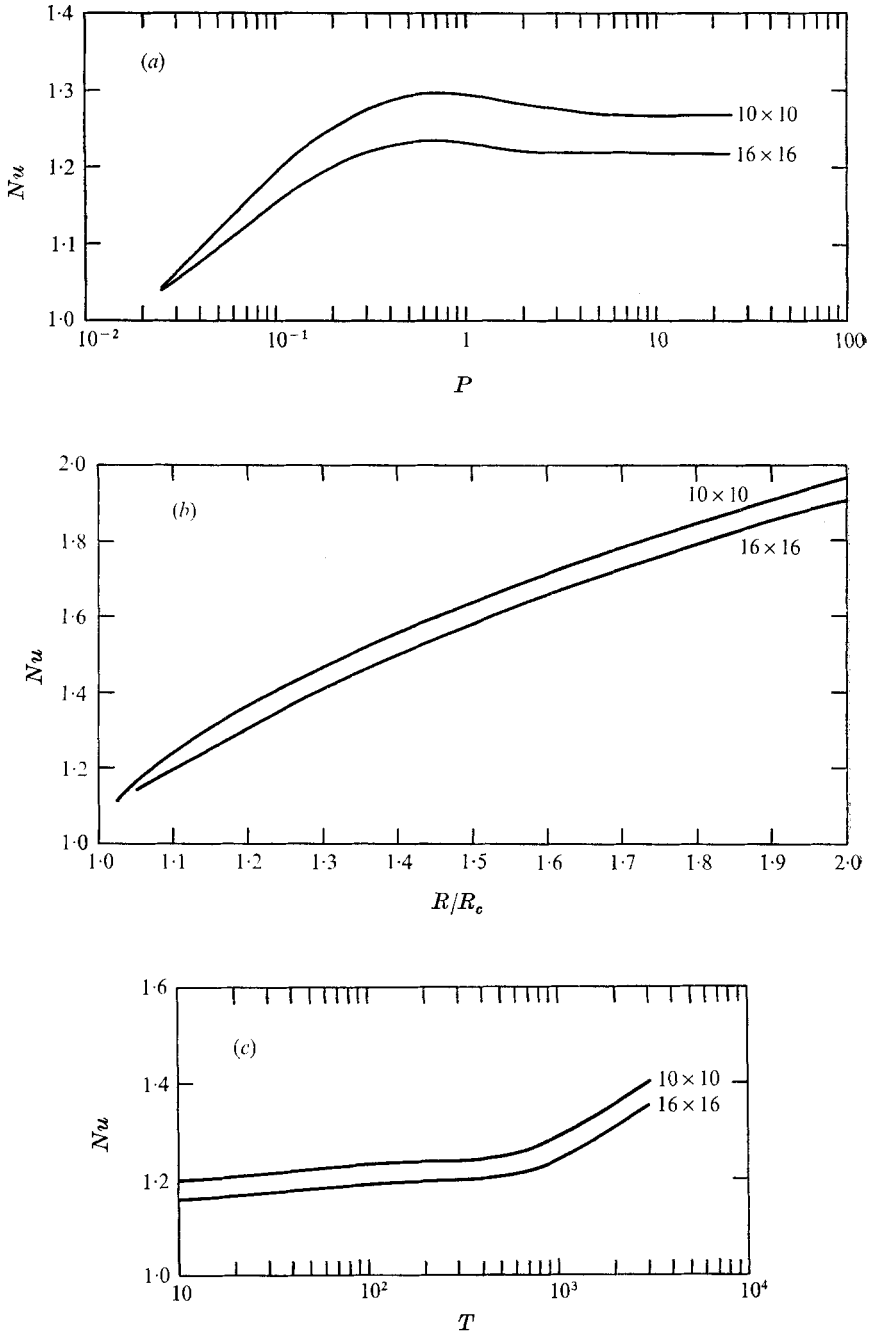

FIGURE 8. Nusselt number (*a*) as function of P for same case as figures 6(*a*) and 7; (*b*) as function of R/R_c for same case as figure 6(*b*); and (*c*) as function of T for same case as figure 6(*c*).

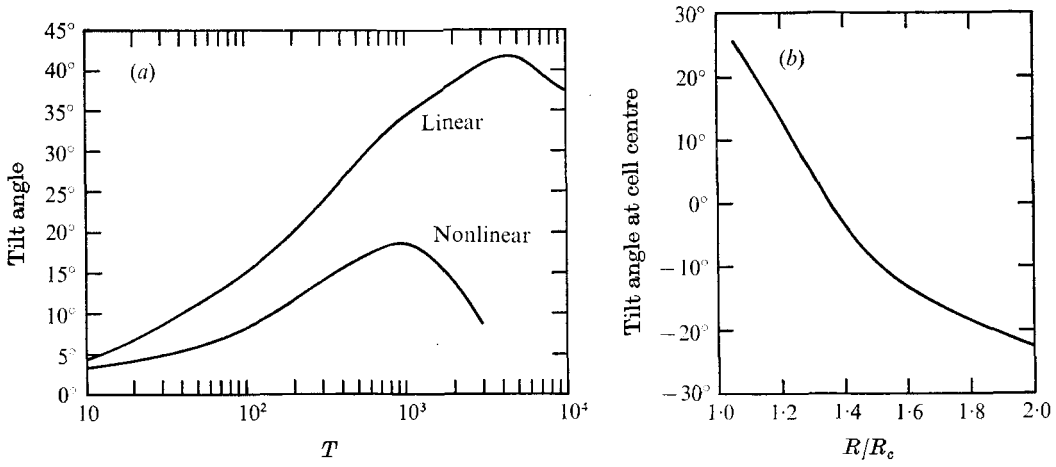

FIGURE 9. Tilt angle of vertical convective cell boundaries at centre of annulus cross-section. (*a*) For both linear and nonlinear cases as function of Taylor number T with $P = 0{\cdot}7$ (air) and $R = 1{\cdot}2R_c(T)$ (as in figures 6(*c*) and 8(*c*)). (*b*) As a function of R/R_c for $T = 2 \times 10^3$, $P = 0{\cdot}7$ (as in figures 6(*b*) and 8(*b*)).

kinetic-energy ratios, presumably because both the numerator and denominator of those ratios change in the same sense as the resolution is changed.

5.5. *Cell structure changes*

As the Taylor number increases, the vertical cell boundaries in the stationary convection tilt more and more away from the position perpendicular to the sides. For example, figure 9(*a*) shows the tilt angle for the linear solutions with $P = 0{\cdot}7$ and $R = 1{\cdot}2R_c$ (positive angles represent clockwise tilt when viewed from above). Through the range $T < 3 \times 10^3$, where stationary convection is preferred, the angle increases monotonically to almost 45°. Now, in the nonlinear case, the differential rotation and meridional circulation that develop strongly reduce the amount of this tilt. For example, by $T = 2 \times 10^3$, the tilt is almost 30° less in the nonlinear case. This is true even though the amount of energy in the differential rotation is only about 4 % of the energy in the same component of cell motion. In addition, the tilt angle continues to decrease as R/R_c is increased even beyond the peak relative kinetic energy in the differential rotation. Figure 9(*b*), for example, shows that, for $T = 2 \times 10^3$ and $P = 0{\cdot}7$, the angle actually reverses near $R = 1{\cdot}4R_c$, reaching $\sim -20°$ by $R = 2{\cdot}0R_c$. What is in fact happening is that the mean circulations are bending the cell boundaries from a slanted straight line into an S shape (figure 10), which is indicative of the horizontal shearing action of the induced differential rotation. Figure 10 shows this effect where it is strongest, namely, at the midlevel of the annulus. A plot of the boundary in an x, z plane (not shown) would indicate a bulge in the $+x$ direction in the outer half of the annulus, and an opposite bulge in the inner half, corresponding to the action of the vertical shear in the differential rotation.

That the distortion of the cell boundaries by the mean circulations, particularly the differential rotation, continues to increase with R/R_c even after the relative

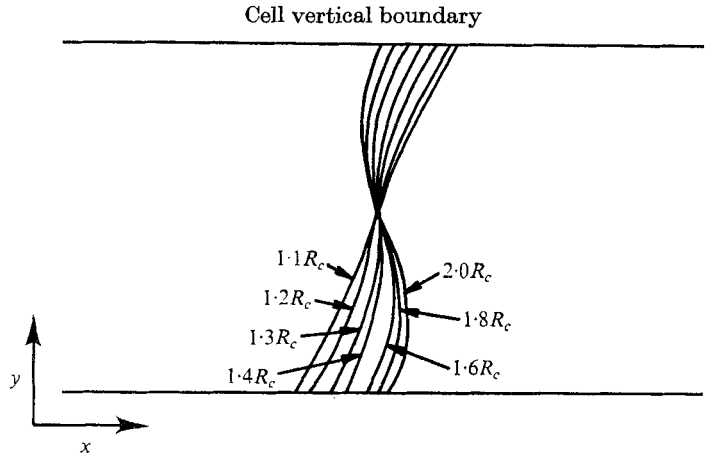

FIGURE 10. Profiles of cell vertical boundary as function of R/R_c at mid-level of annulus. $T = 2 \times 10^3$, $P = 0{\cdot}7$, $k = 3{\cdot}7$.

peak in differential rotation amplitude is passed is due to the fact that distortion of the cell boundaries is related to the absolute value of u_0, which is displacing them up- and downstream. This displacement effect is strongest at midlevels because the differential rotation is largest there and because the cell motion is essentially vertical there; columns of rising and sinking warm and cold fluid are simply displaced up- and downstream.

In sum, then, the reaction of the mean circulation on the cells is to distort their boundaries qualitatively like the profiles of differential rotation. From linear theory, a mean shear would tend to favour cells elongated in the x direction, but since our x wavenumber k is fixed it would be difficult for this to show up unless longitudinal rolls ($k = 0$) were strongly favoured. In the parameter range studied no transition to longitudinal rolls was found. It is possible, of course, that, with subharmonic modes allowed, these might tend to be excited more by the presence of the shear, and, with sufficient shear, actually become larger in amplitude than the originally most unstable mode.

5.6. *Overstability*

As suggested from figure 5, finite amplitude overstable convection in the annulus should lead to an oscillatory differential rotation. In figure 5, we can see that, at time steps 3100 and 3300, momentum is being transported horizontally towards the outer rim just as in the stationary convection cases studied earlier (figure 1 (*c*)). The vertical momentum transport is also similar (figure 1 (*d*)). However, with the rotation of the velocity vectors, by step 3500, the bulk of the horizontal transports has been reversed and is now toward the inner rim. This remains true for step 3700. The vertical transports are also reversed. By step 3900, the sense of transport is reversed again. In the cells, the evolution from step 3100 to step 4100 represents slightly less than half a period, as evidenced by the fact that the two sets of arrows are almost 180° out of phase with each other.

The evolution of the mean circulations due to this overstable convection

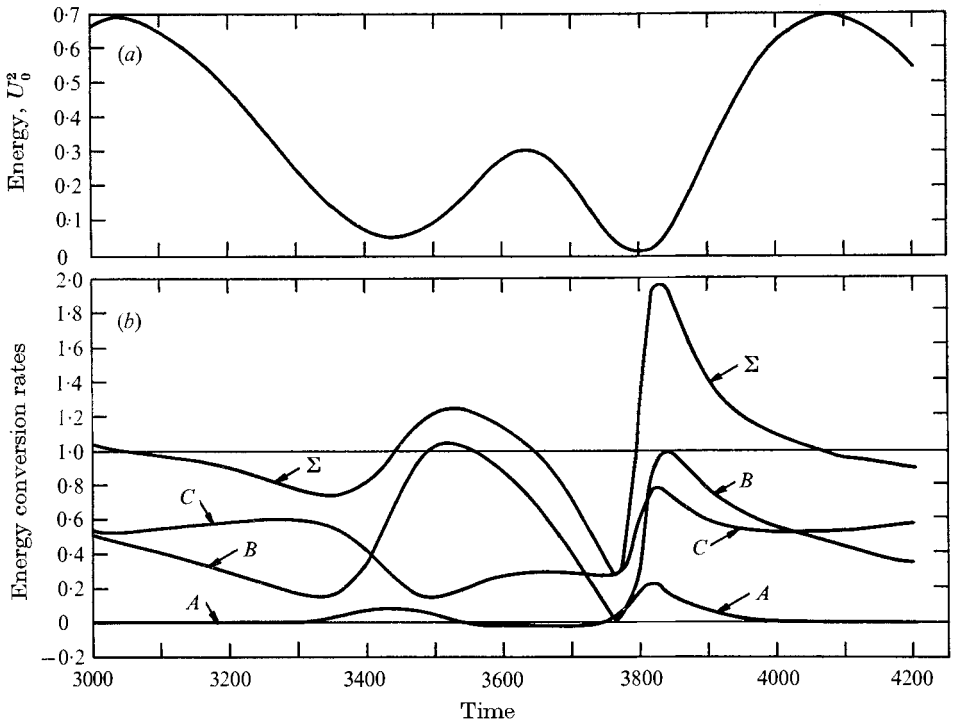

FIGURE 11. (*a*) Differential-rotation energy and (*b*) energy conversion rates (lower figure) for half-cycle of an overstable convective oscillation with $T = 10^4$, $R = 5700$, $P = 0{\cdot}7$, $k = 2{\cdot}9$ (as in figure 5).

would require many figures to describe in detail, so we content ourselves here with a qualitative description of the structure together with a closer examination of the energetics of the cycle, which are shown in figure 11, for the same phases as the cell horizontal velocities shown in figure 5.

Around time step 3040, the momentum transports have built up to its peak in energy a differential-rotation profile very much like figure 1(*a*), with faster rotation in the outer half of the annulus and slower rotation in the inner half. This peak (see figure 11(*a*)) then falls off, as the horizontal and vertical transports change direction, until a *lesser* peak of differential rotation of the opposite sense is built up by around step 3600. This is then destroyed by the momentum transport reversing again and building up the larger peak of differential rotation with fast flow in the outer half, by about step 4080. This pattern then repeats about every 1040 steps for the particular case studied. The meridional circulation also changes, but is weaker in energy than the differential rotation by a factor of 300 or so, so we do not discuss it in detail.

The maintenance of the energy in the differential rotation is shown in figure 11(*b*). We see that the Coriolis forces acting on the meridional circulation have a very small effect at all phases of the cycle. The work is done almost entirely by the Reynolds stresses. The horizontal and vertical transport successively tear down one peak and build up the next, tearing down when

$\Sigma = B + C + A$ is less than unity (the frictional loss rate) and building up when greater than unity. We note, however, that these integrals are never actually negative during any part of the cycle. In other words, the *net* flux of momentum is always *up* the gradient of differential rotation, even though those gradients are continuously evolving, and periodically changing sign. At some times during the cycle, however, there is downgradient momentum flux in some parts of the annulus cross-section, and this leads to the reversal in the sense of differential rotation.

From figure 11, it is clear that if we were to average the velocities and stresses over a cycle, we would get non-zero values; that is, the oscillation is not symmetric about zero. This is a natural consequence of the overstable convection. As we said earlier, in the linear case there are two overstable modes which propagate in opposite directions. We may therefore think of these as having frequencies $\pm\omega$. The induced axisymmetric circulations arise from the Reynolds and thermal stresses due to self-coupling and cross-coupling of these modes. The self-coupling gives rise to stresses that are independent of time which force the non-zero time-mean axisymmetric circulations, while the cross-coupling yields stresses and therefore axisymmetric circulations with period 2ω which produce the variations seen in figure 11. The total induced circulations, then, are a combination of these.

In these finite amplitude overstable solutions, the nature of overstability as an inertial oscillation comes through quite clearly, in that, while the kinetic energy in the individual components of horizontal motion oscillates from essentially zero to peak amplitudes, the total kinetic energy varies by only about 7 % through the cycle. The Nusselt number varies only between about 1·36 and 1·42 for the particular example studied. The peak kinetic energy in the differential rotation (at the major peaks in the cycle) is approximately 14 % of the energy in an average horizontal component of motion.

6. Concluding remarks

To the writer's knowledge, the results presented above represent the first nonlinear study of convection in a rotating annulus in which the bottom heating is uniform. We have fairly systematically surveyed nonlinear cases near the critical Rayleigh number for stationary convection, and presented what we believe to be a typical example of the overstable case. Clearly, however, much more could be done. Increasing R further above the critical value requires the presence of additional modes and eventually more points in the cross-section grid. The transition between stationary and overstable nonlinear convection should be studied, as well as the production of other modes due to nonlinear effects.

The original motivation for I and this study was the problem of the solar differential rotation. In this context, our results are in some respects disappointing. We did achieve fast rotation of the outer half of the annulus, corresponding roughly to the equatorial acceleration on the Sun, but the amplitude of this low latitude 'acceleration' is, for the Taylor numbers we considered, rather small compared with that of the forcing cells. Solar observations, e.g.

Howard & Harvey (1970), Howard (1971), indicate the cells should be in fact no larger, and perhaps smaller, in amplitude than the differential rotation. Even so, our model did show considerable distortion of the cell boundaries into shapes roughly following the differential-rotation profile, some indirect evidence for which can be seen in the solar magnetic fields (Starr & Gilman 1965; Simon & Weiss 1968; and others). The relative amplitude possible in the differential rotation compared with that in the cells does increase with T, but we also get overstability and resulting large oscillations in the differential rotation. This probably does not happen in solar equatorial regions, where rotation is nearly perpendicular to gravity rather than parallel to it as in our model. Instead we shall get a convectively excited Rossby wave, along the lines modelled by Busse (1970), Durney (1970, 1971) and Gilman (1972).

The results we have presented should be confirmable by laboratory experiment. Except for the initial scans in Prandtl number, we have concentrated on the case $P = 0{\cdot}7$, i.e. air, because it is a common fluid for which the Reynolds stress and differential-rotation effects should be significant. Water ($P = 6{\cdot}8$), which is perhaps easier to use experimentally, will unfortunately show much smaller relative differential rotation.

The writer wishes to express his thanks to Mr Jack Miller, of the NCAR Computing Facility, for his careful programming of all computations reported in this paper.

REFERENCES

Busse, F. 1970 *Astrophys. J.* **159**, 629.

Chandrasekhar, S. 1961 *Hydrodynamic and Hydromagnetic Stability.* Oxford University Press.

Davies-Jones, R. P. & Gilman, P. A. 1971 *J. Fluid Mech.* **46**, 65.

Durney, B. 1970 *Astrophys. J.* **161**, 1115.

Durney, B. 1971 *Astrophys. J.* **163**, 353.

Gilman, P. A. 1972 *Solar Phys.* In press.

Howard, R. 1971 *Solar Phys.* **16**, 21.

Howard, R. & Harvey, J. 1970 *Solar Phys.* **12**, 23.

Rossby, H. T. 1969 *J. Fluid Mech.* **36**, 309.

Simon, G. & Weiss, N. O. 1968 *Z. Astrophys.* **69**, 435.

Starr, V. P. & Gilman, P. A. 1965 *Tellus*, **17**, 334.

Stuart, J. T. 1958 *J. Fluid Mech.* **4**, 1.

Williams, G. P. 1969 *J. Fluid Mech.* **37**, 727.